Modification of lipid rafts by extracellular vesicles carrying HIV-1 protein Nef induces redistribution of amyloid precursor protein and Tau, causing neuronal dysfunction

Modification of lipid rafts by extracellular vesicles carrying HIV-1 protein Nef induces redistribution of amyloid precursor protein and Tau, causing neuronal dysfunction

Michael Ditiatkovski[1,‡], **Nigora Mukhamedova**[1,‡], **Dragana Dragoljevic**[1], **Anh Hoang**[1], **Hann Low**[1], **Tatiana Pushkarsky**[2], **Ying Fu**[1], **Irena Carmichael**[3], **Andrew F. Hill**[4], **Andrew J. Murphy**[1], **Michael Bukrinsky**[2], **and Dmitri Sviridov**[1,5,*]

From the [1]Baker Heart and Diabetes Institute, Melbourne, Victoria, Australia, the [2]Department of Microbiology, Immunology and Tropical Medicine, George Washington University School of Medicine and Health Sciences, Washington, D.C., USA, the [3]Department of Micro Imaging, Monash University, Melbourne, Victoria, Australia, the [4]Department of Biochemistry and Genetics, Louisiana Trobe Institute for Molecular Science, Louisiana Trobe University, Bundoora, Victoria, Australia, and the [5]Department of Biochemistry and Molecular Biology, Monash University, Clayton, Victoria, Australia

Edited by Dennis R. Voelker

HIV-associated neurocognitive disorders (HANDs) are a frequent outcome of HIV infection. Effective treatment of HIV infection has reduced the rate of progression and severity but not the overall prevalence of HANDs, suggesting ongoing pathological process even when viral replication is suppressed. In this study, we investigated how HIV-1 protein Nef secreted in extracellular vesicles (exNef) impairs neuronal functionality. ExNef were rapidly taken up by neural cells *in vitro*, reducing the abundance of ABC transporter A1 (ABCA1) and thus cholesterol efflux and increasing the abundance and modifying lipid rafts in neuronal plasma membranes. ExNef caused a redistribution of amyloid precursor protein (APP) and Tau to lipid rafts and increased the abundance of these proteins, as well as of $A\beta_{42}$. ExNef further potentiated phosphorylation of Tau and activation of inflammatory pathways. These changes were accompanied by neuronal functional impairment. Disruption of lipid rafts with cyclodextrin reversed the phenotype. Short-term treatment of C57BL/6 mice with either purified recombinant Nef or exNef similarly resulted in reduced abundance of ABCA1 and elevated abundance of APP in brain tissue. The abundance of ABCA1 in brain tissue of HIV-infected human subjects diagnosed with HAND was lower, and the abundance of lipid rafts was higher compared with HIV-negative individuals. Levels of APP and Tau in brain tissue correlated with the abundance of Nef. Thus, modification of neuronal cholesterol trafficking and of lipid rafts by Nef may contribute to early stages of neurodegeneration and pathogenesis in HAND.

HIV-associated neurocognitive disorders (HANDs) include three levels of neurocognitive dysfunction in HIV infection: asymptomatic neurocognitive impairment, mild neurocognitive disorder, and HIV-associated dementia (1, 2). Effective treatment of HIV infection has reduced the rate of progression and severity of HAND symptoms, but the overall prevalence of HAND (up to 50% of HIV-infected subjects) has remained unchanged (1, 3, 4). With aging of HIV-infected population

and dramatically extended life expectancy of people living with HIV (PLWH), this condition constitutes a significant health problem.

HAND has clinical features characteristic for a neurodegenerative disorder: a spectrum of declining cognitive functions, behavioral changes, and motor impairment. Pathologically, there may or may not be focal damage to the gray matter, and there are abnormalities in the white matter (4). Overall, HAND is consistent with the definition of a neurodegenerative disease as a condition with progressive neuronal damage and chronic loss of neurons (4). In treated patients, however, pathological features may be modest, pointing to more subtle changes to the synaptodendritic architecture manifesting in functional impairment. However, the pathogenetic mechanisms of neural impairment in PLWH are not fully understood.

Cholesterol metabolism and dysregulation of lipid rafts were shown to play a key role in pathogenesis of neural damage in many neurodegenerative diseases, such as Alzheimer's disease (AD), Parkinson's disease, and prion diseases (5–7). High abundance of rafts in neurons is causally involved in neural damage (8). Replication of HIV critically depends on modification of host cholesterol metabolism and lipid rafts through the action of HIV-1 protein Nef (9). Nef reduces the level of the cellular cholesterol transporter ABCA1 inducing accumulation of intracellular cholesterol and overabundance and pathological changes in lipid rafts (10). We recently demonstrated that changes in ABCA1 and lipid rafts inflicted by HIV Nef in macrophages were almost identical to those found in neurons infected by prions (11). Cells do not need to be infected with HIV to be affected by Nef, because Nef is secreted from HIV-infected cells in extracellular vesicles (EVs). These have the same effect on cholesterol metabolism in "bystander" cells in uninfected tissues as Nef in HIV-infected cells (12, 13). Nef-containing EVs ("extracellular" Nef, exNef) were found in relatively high levels in blood and, importantly, in the CSF of HIV-infected subjects treated with anti-retroviral therapy (ART) (14–16). Several studies have suggested a role for systemically available Nef in pathogenesis of HAND, but the proposed mechanisms assumed direct neurotoxicity (16–18). Although

direct toxicity of Nef has been demonstrated *in vitro* (17, 19, 20), the level of toxicity of very low concentrations of Nef found in ART-treated subjects is unlikely to be a primary mechanism of neural damage. In this study, we tested a hypothesis that Nef-containing EVs contribute to the neuronal damage by reorganizing lipid rafts and causing accumulation of amyloidogenic proteins in these membrane domains.

Results

Uptake of Nef-containing EVs

In this study, we used EVs produced by HEK293 cells transfected with either Nef or GFP (control). As established in our previous studies (13, 21), these EVs, designated as exNef and exGFP, respectively, have predominant sizes of 120–150 nm, were positive for ALIX, tetraspanin CD63 and Hsp70 (cytosolic marker), and negative for cytochrome *c*, thus satisfying International Society for Extracellular Vesicles criteria for extracellular vesicles (22). They did not contain Nef-coding mRNA (13). ExNef contained Nef at an average concentration of 0.5 ng Nef/1 μg of total EV protein (13), Nef content of EVs was measured separately for each batch, and control exGFP was added to cells in total EV protein concentration matching that of exNef. Unless indicated otherwise, the concentration of exNef used in this study was 0.4 ng/ml of Nef, which is lower than the concentration of Nef detected in the blood of ART-treated individuals with undetectable viral load (15, 23). It was demonstrated in our previous study that the effects of EVs produced by Nef-expressing cells on cholesterol metabolism and lipid rafts are similar to the effects of EVs produced by HIV-infected myeloid cells, whereas EVs from cells infected with ΔNefHIV did not have such effects (13).

To determine whether differentiated SH-SY5Y human neuroblastoma cells could take up the EVs, we labeled EVs with fluorescent dye PKH67. EV uptake was slow over the first 4 h but increased in a linear fashion over the following 4 h (Fig. 1, *A* and *B*). No fluorescence was found inside the cells when BSA instead of EVs was added to the stain solution and incubated with cells for 8 h (Fig. 1*A*, *last panel*), suggesting that EVs were taken up by SH-SY5Y cells. To determine whether EVs could deliver Nef into cells, we incubated EVs containing Nef tagged with GFP (exGFP-Nef) with the cells for 24 h and used anti-GFP antibody to enhance the detection signal. GFP-Nef was detected inside the cells after a 24-h incubation and intracellular abundance of Nef continued to rise for at least another 24 h (Fig. 1, *C* and *D*). Thus, exNef was actively taken up by SH-SY5Y cells delivering Nef to the cell interior.

Nef-containing EVs modify cholesterol metabolism and lipid rafts in neural cells

We have previously demonstrated that Nef expressed in macrophages infected with HIV-1 or transfected with heterologous Nef, as well as delivered to cells by incubation with the recombinant Nef or Nef-containing EVs, reduces the abundance of ABCA1 and the rate of cholesterol efflux in macrophages (10, 13). Similar effects were observed when we tested the effects of 48 h of incubation with exNef (final concentration, 0.4 ng/ml) on SH-SY5Y neural cells. The abundance of

total and cell surface ABCA1 and the rate of cholesterol efflux were reduced by 35% (*n* = 3) and 3-fold, respectively (Fig. 2, *A* and *B*). Another effect of Nef was elevation of the abundance of lipid rafts. Incubation of exNef with SH-SY5Y cells for 48 h also led to elevation of the abundance of lipid rafts as determined by confocal microscopy after staining with fluorescently tagged cholera toxin subunit B (CTB) (Fig. 2, *C* and *D*). To ensure that the effects of exNef can be attributed to Nef and not to a Nef-induced factor that may be carried by EVs produced by Nef-expressing cells, we incubated SH-SY5Y cells with myristoylated recombinant Nef (final concentration, 100 ng/ml). Recombinant Nef also caused elevation of the abundance of lipid rafts as determined by CTB binding and confocal microscopy (Fig. 2*E*) or flow cytometry (Fig. 2*F*), although the effects were less pronounced than with exNef and required higher concentration of Nef, similar to what was seen with macrophages (13). Next, we labeled cells with [³H]cholesterol and isolated lipid rafts from plasma membranes using density gradient centrifugation. Fractions containing the highest concentrations of [³H]cholesterol and lipid raft marker flotillin-1 were designated as lipid rafts; both markers co-distributed along the density gradient (Fig. 2, *G* and *H*). When we compared lipid rafts isolated from cells treated with exNef and exGFP, we found that lipid raft fractions from cells treated with exNef contained more cholesterol and more flotillin-1 than fractions from cells treated with exGFP. Furthermore, the density of the fractions containing maximum amounts of cholesterol and flotillin-1 was lower (lighter fractions) in cells treated with exNef (Fig. 2, *G* and *H*). These findings are consistent with lipid rafts in cells treated with exNef being more abundant and possibly bigger.

ExNef causes accumulation of APP and Tau in lipid rafts and induces inflammation

Elevation of the abundance of lipid rafts may cause elevation of the abundance of lipid raft-associated amyloidogenic proteins. We tested the effect of exNef on the abundance of several amyloidogenic proteins in cell lysates and found elevated abundance of APP and Tau in cells treated with exNef (Fig. 3, *A* and *B*). This was confirmed with an independent method, confocal microscopy. Staining for APP and Tau on cell membranes was elevated in cells treated with exNef as compared with cells treated with exGFP (Fig. 3, *C* and *D*). We then used ELISA to evaluate the amount of amyloid Aβ_{42}. The abundance of Aβ_{42} in cells treated with exNef tripled compared with cells treated with exGFP (Fig. 3*E*); the abundance of Aβ_{42} in the medium after 24 and 48 h of incubation was below the detection limit of the method. There was no difference in the abundance of α-synuclein and L-neurofilament in the cells (not shown).

Several reports indicated that an essential step in formation of Tau microfilaments is hyperphosphorylation of Tau (24, 25). Therefore, we assessed the abundance of phosphorylated Tau (pTau) in the plasma membranes of SH-SY5Y neural cells using Western blotting. Treatment of cells with exNef resulted in elevation in the abundance of pTau in parallel with increased total abundance of Tau (Fig. 3*F*). Interestingly, we also found that treatment with exNef increased the abundance of total and phosphorylated of ERK 1/2 (Fig. 3*F*), which may contribute, on
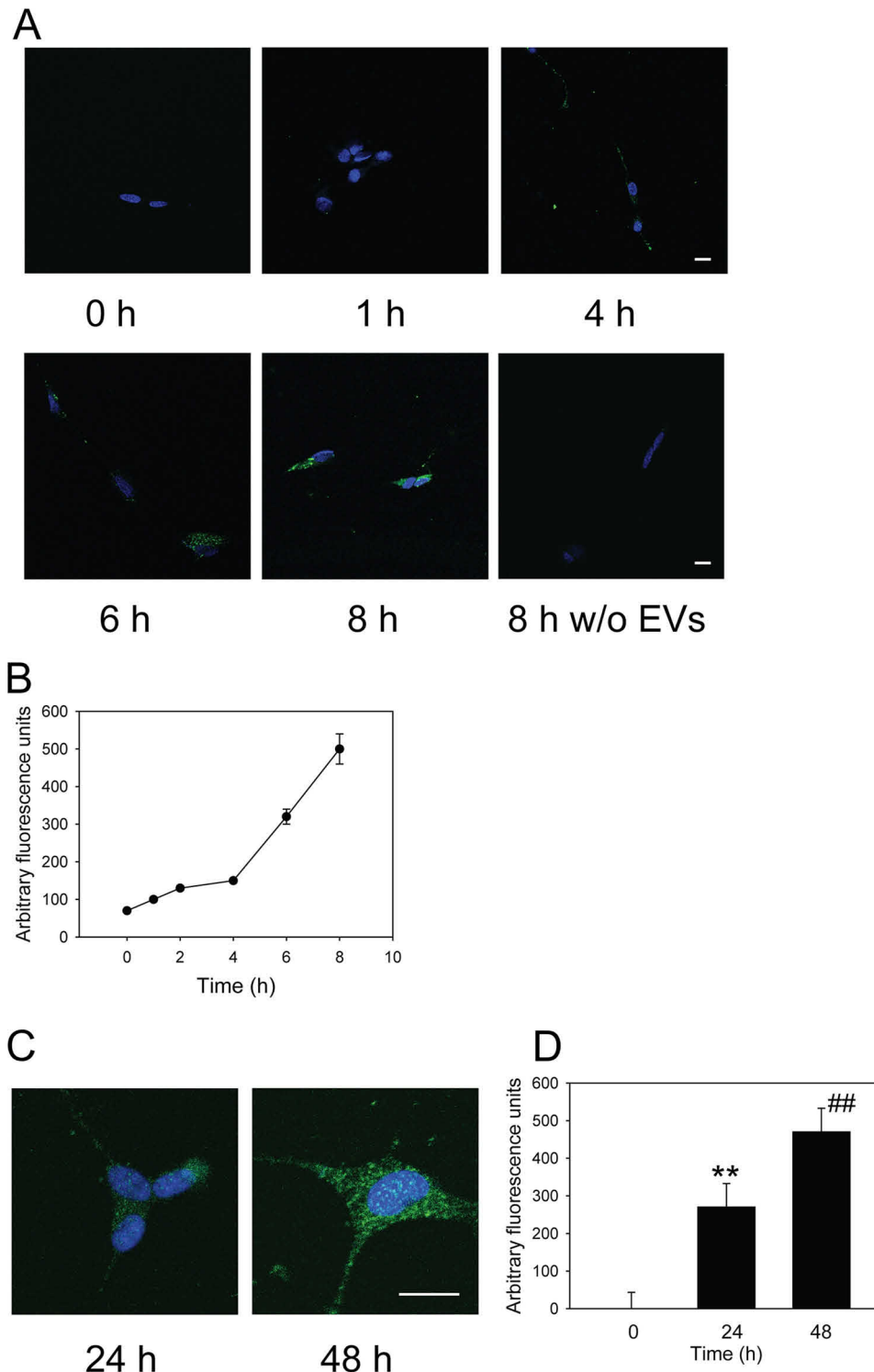
Figure 1. Nef-containing EVs deliver Nef to SH-SY5Y neural cells. *A* and *B*, time course of EV uptake quantitated by confocal microscopy. Confocal images (*A*) and quantitation (*B*). Means ± S.D. are shown. *C*, visualization of Nef-GFP inside the cells after exposure to exNef-GFP (5 μg/ml of EV protein) after staining with anti-GFP antibody. *D*, mean fluorescence intensity of the abundance of Nef in the cell interior after incubation with exNef-GFP for the indicated periods of time. Means ± S.D. are shown. **, $p < 0.01$ *versus* 0-h time point; ##, $p < 0.01$ *versus* 24-h time point. *Scale bars*, 10 μm.

the one hand, to hyperphosphorylation of Tau (26), and, on the other hand, to the elevated inflammatory status characteristic for brains of HIV-infected persons. The increased pro-inflammatory and pro-apoptotic signaling induced by exNef was further supported by elevation in phosphorylation of p38 MAPK in cells treated with exNef (Fig. 3*G*).

Next, we assessed the cellular localization of APP and Tau in SH-SY5Y cells using confocal microscopy. Localization of APP and Tau in the SH-SY5Y cells is shown in Fig. 4 (*A* and *B*, respectively); most of APP and Tau localized at the plasma membranes and co-localized with lipid rafts. The co-localization of these proteins with lipid rafts was measured as Manders'
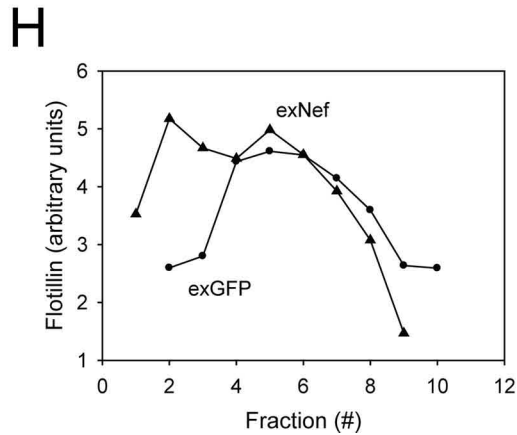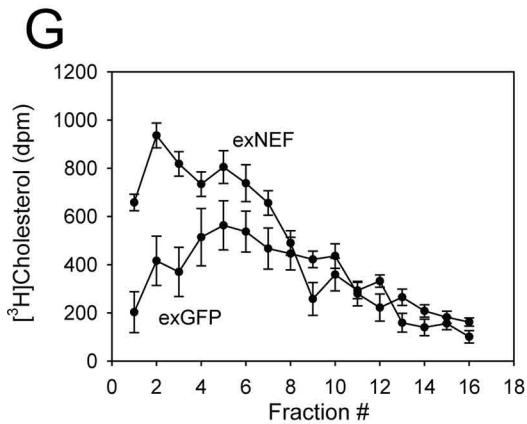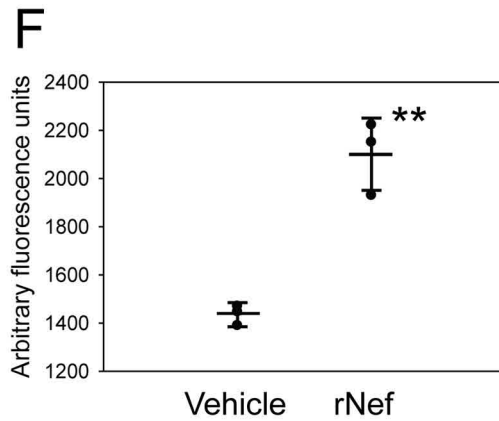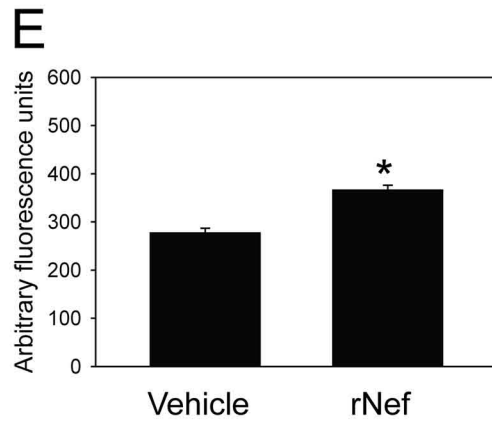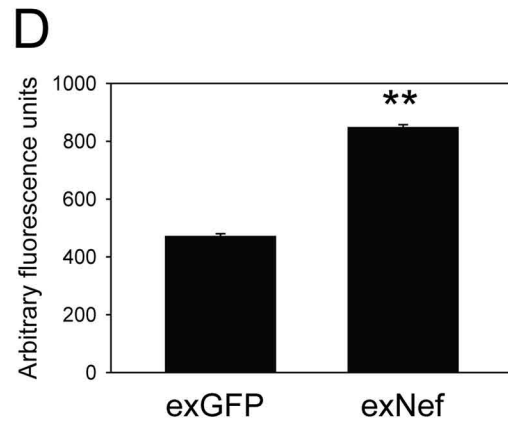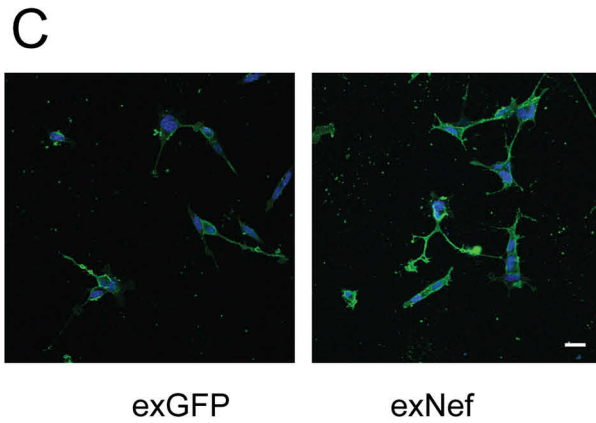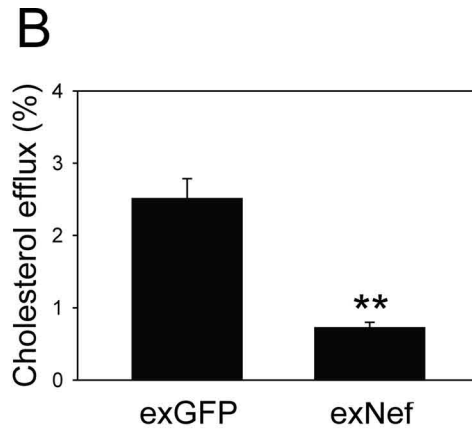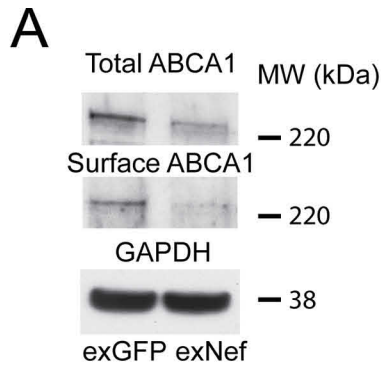
co-localization coefficient (M2) (27). We found that treatment of cells with exNef increased co-localization of both APP and Tau with lipid rafts (Fig. 4, *A–D*). We then isolated lipid rafts by density gradient centrifugation and determined the abundance of flotillin-1 and APP in individual fractions. Higher abundance of APP was found in lipid raft fractions of cells treated with exNef compared with that of cells treated with exGFP (Fig. 4*E*). We next probed the abundance of flotillin-1, APP, and phosphorylated Tau by Western blotting in combined raft or nonraft fractions. There was considerably higher abundance of flotillin-1 in raft fractions; rafts from exNef-treated cells had more flotillin-1 than rafts from cells treated with exGFP (Fig. 4*F*). All detectable APP was found in raft fractions of exNef-treated cells; APP abundance in nonraft fractions of exNef-treated cells, as well as in both raft and nonraft fractions of exGFP-treated cells, was very low. Phosphorylated Tau was found in both raft and nonraft fractions with higher abundance in exNef-treated cells (Fig. 4*F*). Saribas *et al.* (17) found no effect of Nef expression in SH-SY5Y cells on the level of phosphorylated Tau. However, that study analyzed phosphorylated Tau in cell lysates as opposed to plasma membranes analyzed in our experiments.

ExNef causes neuronal functional impairment

Previously, the neuropathic effects of Nef were attributed to its toxicity at high concentrations. However, when we tested for toxic effects of exNef at concentration and conditions of this study, exNef did not cause elevation of the rates of necrosis (Fig. 5*A*) or apoptosis (Fig. 5*B*) in SH-SY5Y cells.

Two functional assays were employed to test whether exNef causes functional impairment in neural cells. First, we tested excitotoxicity by measuring susceptibility of SH-SY5Y cells to glutamate-induced apoptosis. This pathway of cell injury plays an integral role in pathogenesis of a number of neurodegenerative disorders, including AD and Parkinson's disease (28, 29). Consistent with lack of general toxicity, exNef did not cause an elevation of the proportion of dead cells in culture in the absence of glutamate (Fig. 5*C*). However, when treated with 50 μM glutamate, the apoptosis of neural cells pretreated with exNef was significantly increased (Fig. 5*C*). Second, we tested the activity of acetylcholine esterase (AChE), a measure of cholinergic hypofunction, which was linked to cognitive decline (30). The activity of AChE in cells pretreated with exNef was significantly higher than in cells pretreated with exGFP (Fig. 5*D*).

To confirm that functional changes in neural cells caused by exNef were due to modification of lipid rafts, we tested whether reversal of the effects on lipid rafts would also reverse functional impairment. We used methyl-β-cyclodextrin (MβCD), a

nonspecific cholesterol acceptor well-known for its capacity to disrupt lipid rafts. Treatment with 0.25 mM of MβCD for 60 min, a condition previously reported as sufficient to disrupt rafts without causing toxic effects on cells (31), effectively reversed the elevation of the abundance of lipid rafts caused by exNef (Fig. 6, *A–C*). Interestingly, MβCD had little effect on the abundance of rafts in exGFP-treated cells (Fig. 6, *A–C*). The abundance of both APP and Tau was elevated in exNef-treated cells, but treatment with MβCD reduced it to an undetectable level both in exGFP and exNef-treated cells (Fig. 6, *A and B*). AChE activity elevated by treatment with exNef was reduced by treatment with MβCD to the level similar to that seen in cells treated with exGFP, with little effect on exGFP-treated cells. (Fig. 6*D*).

Nef causes reduction of ABCA1 and accumulation of APP in brains in vivo

To confirm our findings in an *in vivo* setting, we injected C57Bl/6 mice intravenously with either recombinant myristoylated Nef (rNef; 50 ng/injection twice a week for 9 days) or vehicle. In another experiment we injected mice intravenously with exNef or exGFP (2 μg EV protein/injection (total 1 ng of Nef), thrice a week for 14 days); in both experimental setups, we analyzed the abundance of several proteins in brain homogenates. When mice were treated with rNef, ABCA1 abundance in the brains was reduced by 25% (Fig. 7*A*), and APP abundance was elevated by 50% (Fig. 7*B*). There was a trend for elevation of the abundance of Tau, but the difference did not reach statistical significance (Fig. 7*C*). A similar profile was seen when mice were treated with exNef. We noted that ABCA1 abundance in the brains was reduced by 25% (Fig. 7*D*), and APP abundance has doubled (Fig. 7*E*). However, there was no difference in the abundance of Tau, and the abundances of L-neurofilament and α-synuclein were slightly reduced (Fig. 7, *F–H*). Thus, short-term treatment with Nef resulted in predicted reduction of ABCA1 abundance and elevation of the abundance of some but not other amyloidogenic proteins.

Level of ABCA1 is reduced and abundance of APP and lipid rafts is increased in brains of patients with HAND

To assess whether HAND is associated with reduced levels of ABCA1 and increased abundance of lipid rafts, APP, and Tau in human brain, we analyzed their abundance in the brain tissue of three groups of subjects. Frozen brain tissues from midtemporal gyrus collected post-mortem from ART-treated HIV-infected patients evaluated for neurocognitive impairment were obtained from National NeuroAIDS Tissue Consortium (NNTC); all samples were anonymized; information about the

Figure 2. ExNef modifies cellular cholesterol metabolism and lipid rafts in SH-SY5Y neural cells. *A*, the effect of exNef (0.4 ng/ml, 48 h) on the abundance of total and cell-surface ABCA1 (Western blotting). *B*, cholesterol efflux to apolipoprotein A-I (final concentration, 20 μg/ml) over 2 h after exposure of cells to exGFP or exNef (0.4 ng/ml for 48 h). Means $\pm$ S.E. are shown on graphs. **, $p < 0.01$, $n = 4$. *C*, the effect of exNef (0.4 ng/ml, 48 h) on the abundance of lipid rafts in SH-SY5Y cells (CTB staining, confocal microscopy). *Scale bar*, 10 μm. *D*, quantitation of the effect of exNef (0.4 ng/ml, 48 h) on the abundance of lipid rafts in SH-SY5Y cells by confocal microscopy (CTB staining, mean fluorescence intensity). **, $p < 0.01$ *versus* exGFP. *E*, quantitation of the effect of recombinant Nef (100 ng/ml, 48 h) on the abundance of lipid rafts in SH-SY5Y neural cells by confocal microscopy (CTB staining, mean fluorescence intensity). *, $p < 0.05$ *versus* vehicle. *F*, quantitation of the effect of recombinant Nef (100 ng/ml, 48 h) on the abundance of lipid rafts in SH-SY5Y neural cells by flow cytometry (CTB staining). *, $p < 0.05$ *versus* vehicle. *G*, amount of [^{3}H]cholesterol in fractions of density gradient centrifugation (from *top* to *bottom*) of plasma membranes from exGFP- or exNef-treated SH-SY5Y neural cells. Means $\pm$ S.D. are shown. *H*, abundance of flotillin-1 in fractions of density gradient centrifugation (from *top* to *bottom*) of plasma membranes from exGFP- or exNef-treated SH-SY5Y neural cells (quantitation of Western blotting). *MW*, molecular mass.
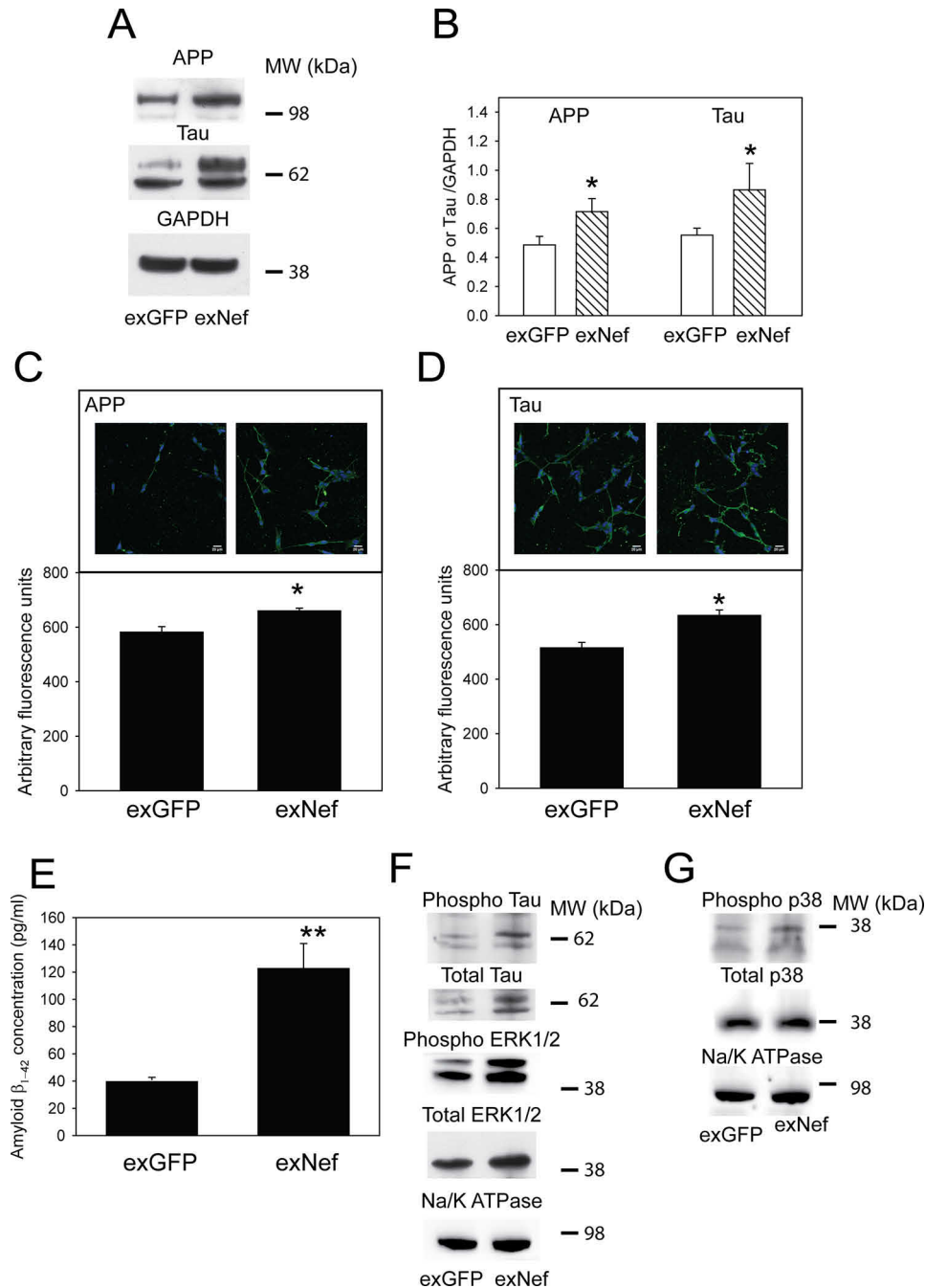
Figure 3. ExNef elevates abundance of APP and Tau and induces inflammation in SH-SY5Y neural cells. *A*, the effect of exNef (0.4 ng/ml, 48 h) on the abundance of total cellular APP and Tau in SH-SY5Y neural cells (Western blotting). Note that GAPDH loading control is the same as in Fig. 2A, because the images were derived from the same Western blotting developed with different antibodies. *B*, quantitation of the effect of exNef (0.4 ng/ml, 48 h) on the abundance of total cellular APP and Tau (densitometry of Western blots). Means ± S.E. are shown. *, $p < 0.05$, $n = 3$. *C*, representative images (*top*) and quantitation (*bottom*) of the effect of exNef (0.4 ng/ml, 48 h) on the abundance of membrane located APP in SH-SY5Y neural cells (confocal microscopy, mean fluorescence intensity). *Scale bar*, 20 μm. Means ± S.E. are shown. *, $p < 0.05$. *D*, representative images (*top*) and quantitation (*bottom*) of the effect of exNef (0.4 ng/ml, 48 h) on the abundance of membrane located Tau in SH-SY5Y neural cells (confocal microscopy, Mean fluorescence intensity). *Scale bar*, 20 μm. Means ± S.E. are shown. *, $p < 0.05$. *E*, quantitation of the effect of exNef (0.4 ng/ml, 48 h) on the abundance of cellular amyloid β_{42} in SH-SY5Y neural cells (ELISA). Means ± S.D. are shown. **, $p < 0.001$. *F*, the effect of exNef (0.4 ng/ml, 48 h) on the abundance of total and phosphorylated Tau and ERK 1/2 (Western blotting). *G*, the effect of exNef (0.4 ng/ml, 48 h) on the abundance of total and phosphorylated p38 MAPK (Western blotting). *MW*, molecular mass.

clinical status of donors was provided by NNTC. Anonymized brain tissue of uninfected controls were obtained from the National Institutes of Health NeuroBioBank. The groups were: (i) HIV-negative subjects (48–57 years old, $n = 3$ (1 male, 2 females)); (ii) HIV-infected subjects without cognitive impairment (32–39 years old, $n = 4$ (all males), all treated with ART), and (iii) HIV-infected subjects with clinical diagnosis of HAND (HIV-associated dementia or minor cognitive and motor disorder, 34–49 years old, $n = 6$ (3 males, 3 females), all treated with ART). We found lower abundance of ABCA1 in brains of HIV-infected subjects with HAND when compared with HIV-negative subjects (Fig. 8, *A* and *B*). The abundance of ABCA1 in brain tissue of HIV-infected subjects without HAND was variable, and despite a trend for being in between the ABCA1 values
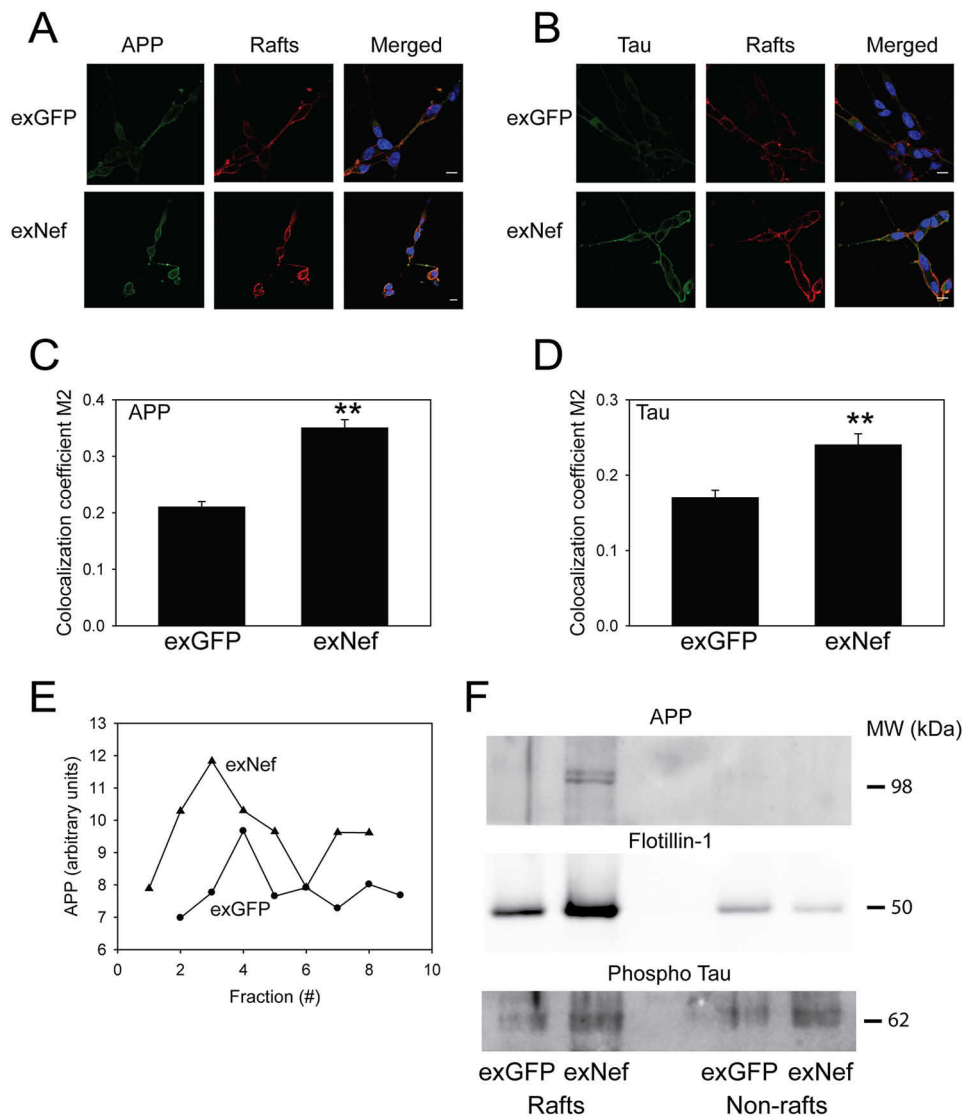
Figure 4. ExNef potentiates relocalization of APP and Tau to lipid rafts in SH-SY5Y neural cells. *A*, the effect of exNef (0.4 ng/ml, 48 h) on the abundance of lipid rafts and relocalization of APP to the plasma membrane in SH-SY5Y neural cells. *Left column*, APP staining; *middle column*, lipid raft staining; *right column*, merged APP/rafts. *Scale bars*, 10 μm. *B*, the effect of exNef (0.4 ng/ml, 48h) on the abundance of lipid rafts and relocalization of Tau to the plasma membrane in SH-SY5Y neural cells. *Left column*, Tau staining; *middle column*, lipid raft staining; *right column*, merged Tau/rafts. *Scale bars*, 10 μm. *C*, quantitation of the effect of exNef (0.4 ng/ml, 48 h) on co-localization of APP and lipid rafts at the plasma membrane. *Bars* show means $\pm$ S.E. of Manders' co-localization coefficient M2. **, $p < 0.01$. *D*, quantitation of the effect of exNef (0.4 ng/ml, 48 h) on co-localization of Tau and lipid rafts at the plasma membrane. *Bars* show means $\pm$ S.E. of Manders' co-localization coefficient M2. **, $p < 0.01$. *E*, abundance of APP in fractions collected after density gradient centrifugation (from *top* to *bottom*) of plasma membranes from exGFP or exNef-treated SH-SY5Y neural cells (quantitation of Western blotting). *F*, abundance of APP, flotillin-1, and phosphorylated Tau in combined raft *versus* nonraft fractions of plasma membranes from exGFP- or exNef-treated SH-SY5Y neural cells. *MW*, molecular mass.

in two other groups, the differences were not statistically significant. There was a trend for higher abundance of APP and Tau in the brains of HIV-infected subjects, but the differences did not reach statistical significance (Fig. 8, *C* and *D*). We found statistically significant higher abundance of lipid raft marker GM1 in brain tissue of HIV-infected subjects without and especially with clinical symptoms of HAND, when compared with HIV-negative subjects (Fig. 8, *E* and *F*). Finally, we assessed whether Nef was present in the brain tissue of HIV-infected subjects. Nef was found in some, but not all brain tissue samples of HIV-infected subjects but not in HIV-negative subjects (Fig. 8*G*). The accuracy of quantitative assessment of the abundance of Nef is limited because of potential differences in immunoreactivity of the antibody with Nef of HIV-1 from different individual patients. With

this limitation in mind, we quantified the images in Fig. 8*G* and calibrated the band density against that of different concentrations of recombinant Nef run in parallel. We found that an approximate concentration of Nef in brain tissue was in the range of 0.05–0.13 ng/mg of total brain protein, a value consistent with the concentration of exNef used in this study. There was trend for correlation between levels of Nef and APP or Tau in HIV+HAND+ group, but correlation did not reach statistical significance (Fig. 8*H*).

Discussion

HAND is a neurodegenerative disorder uniquely associated with HIV infection. In the brain, HIV resides in resident microglial cells and astrocytes, as well as in monocytes/macrophages
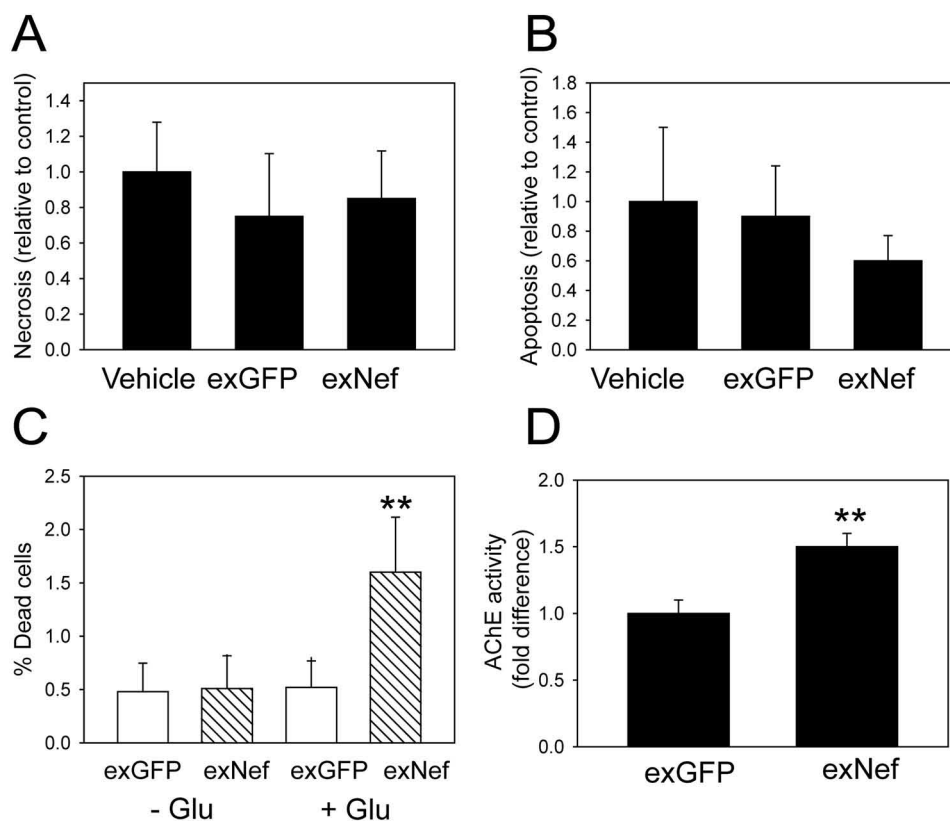
Figure 5. ExNef potentiates functional impairment of lipid rafts in SH-SY5Y neural cells. *A*, the effect of exNef (0.4 ng/ml, 48 h) on necrosis in in SH-SY5Y neural cells. Means ± S.D. are shown. *B*, the effect of exNef (0.4 ng/ml, 48 h) on apoptosis in in SH-SY5Y neural cells. Means ± S.D. are shown, $n = 4$. *C*, the effect of exNef (0.4 ng/ml, 48 h) on the susceptibility of neural cells to glutamate-induced apoptosis (excitotoxicity). Means ± S.D. are shown, $n = 4$. **, $p < 0.001$. *D*, the effect of exNef (0.4 ng/ml, 48 h) on the acetylcholine esterase activity (cholinergic hypofunction) in neural cells. *Bars* show means ± S.E. of fold change relative to exGFP-treated cells, $n = 4$. **, $p < 0.001$.

migrating from blood, but not in neurons (1). It follows that neuronal impairment and eventually neuronal death characteristic for neurodegenerative disorders are not caused directly by the virus but are rather mediated through systemic effects of HIV on bystander cells. HIV infection in the brain persists in treated patients without viremia, forming a *bona fide* HIV reservoir (32), and HIV-infected cells secrete extracellular vesicles containing viral proteins into systemic circulation and into CSF (17, 20). In this study, we tested a hypothesis that one of these proteins, Nef, contributes to the neuronal impairment through its effects on lipid metabolism and lipid rafts.

We have demonstrated that treatment of neural cells with exNef resulted in the uptake of exNef by the cells causing a reduction in the abundance of ABCA1 and the rate of cholesterol efflux. This in turn elevated the abundance and possibly changed the properties of lipid rafts. Two proteins that play a key role in the pathogenesis of AD, amyloid precursor protein and Tau, were also increased in lipid rafts from exNef-treated neural cells. We also detected increased abundance of Aβ and phosphorylation of Tau in cells treated with exNef. This was associated with functional consequences: sensitivity of neural cells to glutamate-induced excitotoxicity was sharply elevated, as was acetylcholinesterase activity, and these effects were reversed by disruption of lipid rafts. Furthermore, treatment of cells with exNef led to increased activation of p38 and ERK

MAPK pathways commonly associated with HIV-related inflammation (33). In C57Bl/6 mice injected with exNef, the abundance of ABCA1 in brain homogenates was significantly reduced, and the abundance of APP increased. EVs were shown to cross the blood–brain barrier (34).

We also observed reduced levels of ABCA1 and increased levels of lipid rafts in brain tissue of HIV-infected human subjects diagnosed with HAND. Tau and APP were also increased in brains samples from HAND patients and appeared to correlate with Nef levels. These findings are consistent with the key initial steps of the proposed hypothesis: exNef impairs ABCA1 and induces formation of lipid rafts in brain cells, leading to accumulation of amyloidogenic proteins in rafts, inflammation, and neuronal dysfunction.

Several hypotheses have been proposed to mechanistically explain the HAND pathogenesis. The most prominent hypothesis suggests that HAND is a result of chronic brain inflammation related to systemic chronic low-grade inflammation that frequently accompanies HIV infection. Elements of inflammation in the brain, *e.g.* monocytosis and astrocytosis, microglial dysfunction and decreased synaptic and dendritic density, can be seen in HIV patients (35). However, although inflammation contributes to pathogenesis of HAND, its role as a primary driving mechanistic basis of HAND has not been proven. Conversely, the role of cholesterol metabolism, and specifically of lipid rafts, in inflammation is well-documented (36). Thus,
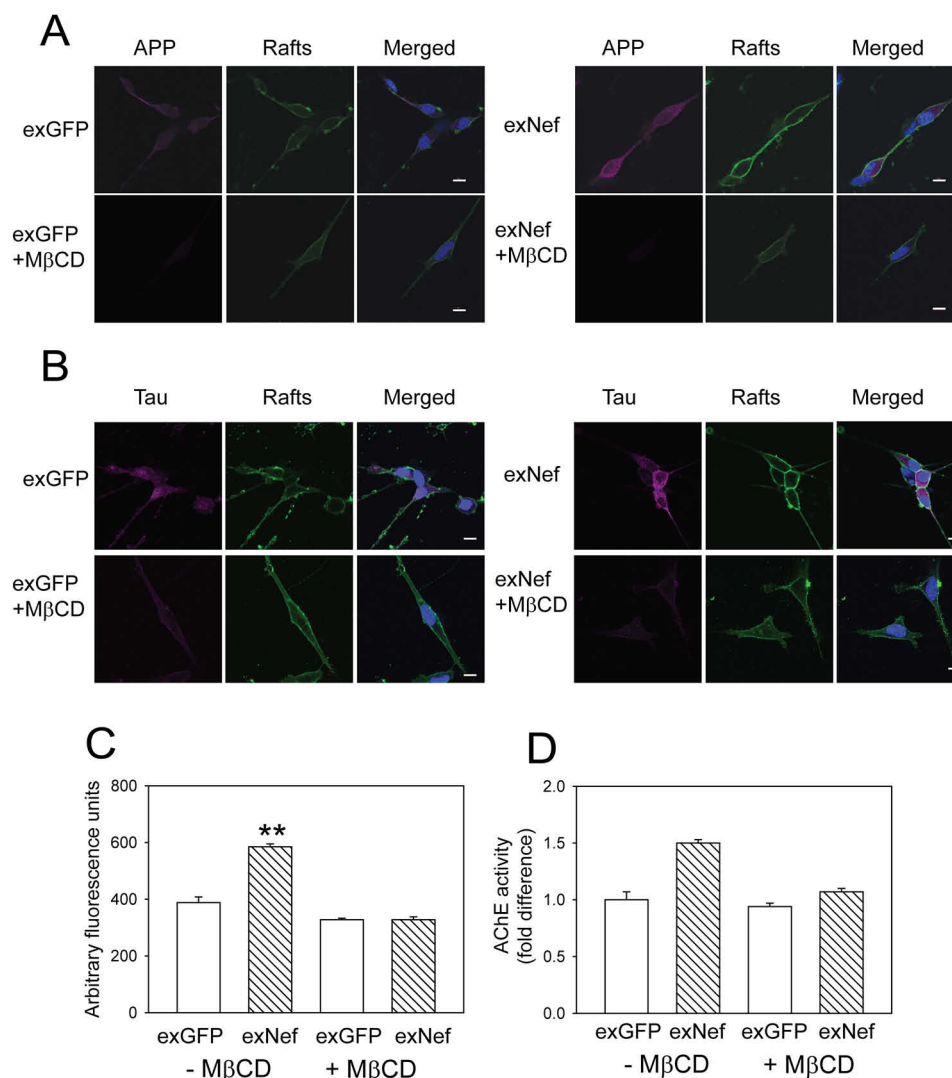
Figure 6. MβCD reverses the effects of exNef on lipid rafts and functional impairment in SH-SY5Y neural cells. *A*, the effect of MβCD (0.25 mM, 60 min) on exNef-induced elevation of the abundance of rafts and APP in SH-SY5Y neural cells. *Scale bar*, 10 μm. *B*, the effect of MβCD (0.25 mM, 60 min) on exNef-induced elevation of the abundance of rafts and Tau in SH-SY5Y neural cells. *Scale bar*, 10 μm. *C*, quantitation Of the effect of MβCD (0.25 mM, 60 min) on exNef-induced elevation of raft abundance in SH-SY5Y neural cells (confocal microscopy, mean fluorescence intensity). **, $p < 0.01$ *versus* exGFP. *D*, the effect of MβCD (0.25 mM, 60 min) on exNef-induced elevation of AChE activity in SH-SY5Y neural cells. Means $\pm$ S.E. are shown, $n = 4$. *, $p < 0.05$ *versus* exGFP; **, $p < 0.01$ *versus* exGFP; #, $p < 0.05$ *versus* exNef in the absence of MβCD.

neurodegeneration and neuroinflammation in HIV infection may have a common cause in lipid raft impairment. Reversing the effect of Nef on lipid rafts may therefore reduce both neurodegeneration and neuroinflammation.

Direct toxicity of proteins secreted by HIV-infected cells may also contribute to neurodegeneration. Apoptosis of neurons is a key feature of late stages of neurodegeneration and several HIV proteins, such as Nef, Env, gp120, and Tat, caused apoptosis in neuronal cells *in vitro* (35). In particular, Nef was identified in brains and CSF of PLWH and was implicated in pathogenesis of HAND (17, 20, 37). However, it remains uncertain whether sufficient quantities of HIV proteins can be produced in the brain under ART treatment to cause apoptosis directly, through toxicity. Notably, apoptosis, like inflammation, may also be secondary to the impairment of cholesterol metabolism and lipid rafts (38). Further, HAND has many similarities with Alzheimer's disease, such as neuroinflammation,

similar transcriptional signatures (39), and increased abundance and changed localization of intracellular Aβ (40). Impairment of cholesterol metabolism and modification of lipid rafts may connect the pathogenesis of both diseases and provide a missing link explaining these similarities. The fact that the proteins accumulating in rafts as a result of treatment with exNef are APP, Aβ, and Tau, but not other amyloidogenic proteins, supports a connection between AD and HAND.

We propose the following hypothetical mechanism of the contribution of exNef to the neurodegeneration cascade (Fig. 9): (i) exNef causes reduction of neuronal ABCA1, leading to increased abundance and modification of lipid rafts (Fig. 9*A*); (ii) accumulation of APP and Tau in modified lipid rafts leads to protein misfolding and aggregation (Fig. 9*B*), and at the same time, aggregated proteins stabilize rafts; (iii) increased abundance and modification of lipid rafts exacerbates inflammatory signaling originating from rafts (Fig. 9*B*); (iv) misfolding of
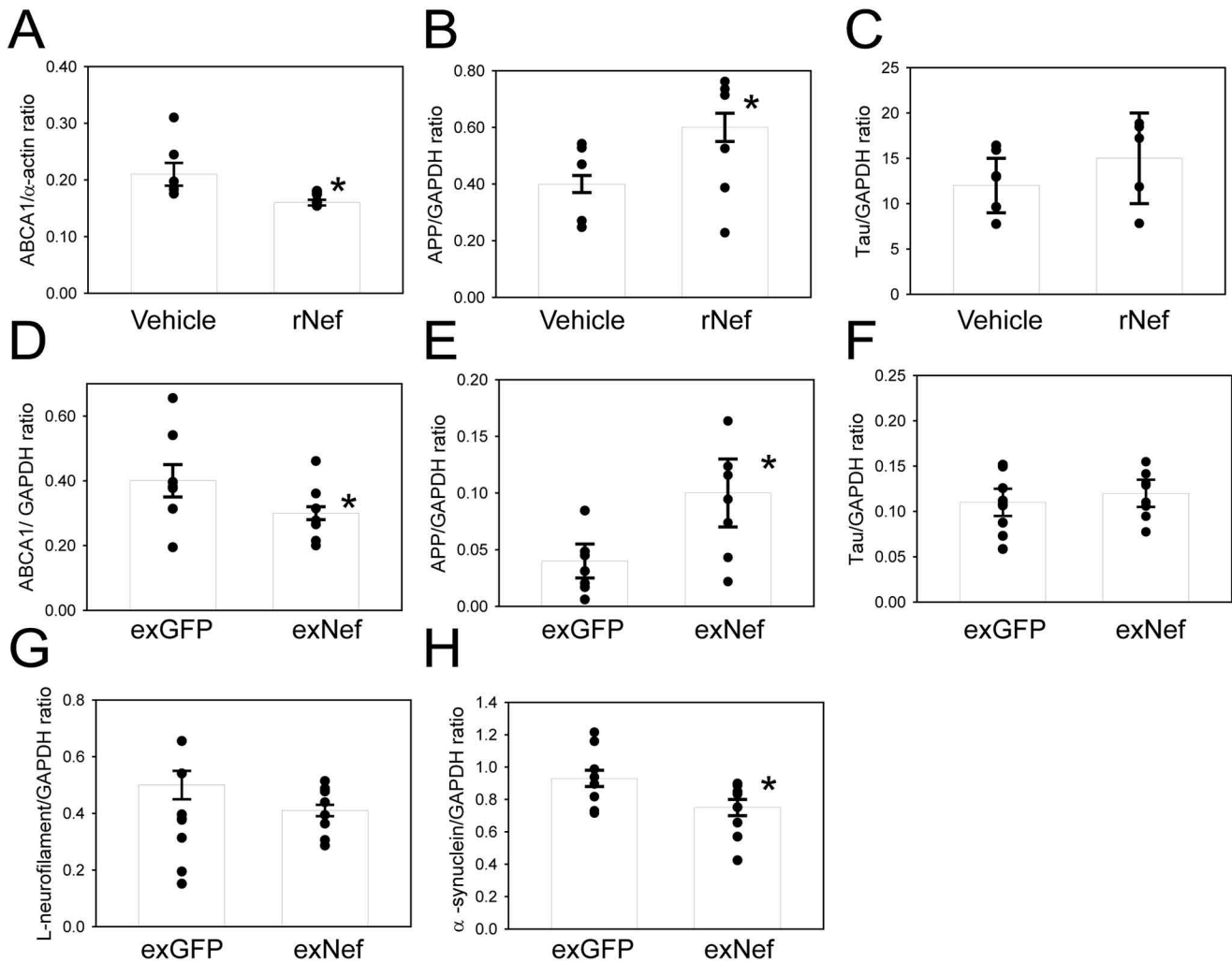
Figure 7. Nef causes reduction of ABCA1 and accumulation of APP in brains *in vivo*. C57Bl/6 mice were injected with either rNef (50 ng/injection twice a week for 9 days) or vehicle (*A–C*) (*n* = 6) or with exNef or exGFP (2 μg of total EV protein per injection, thrice a week for 14 days, *n* = 9) (*D–H*). The brains were excised, homogenized, and subjected to Western blotting. Densitometry was used to analyze the abundance of ABCA1 (*A* and *D*), APP (*B* and *E*), Tau (*C* and *F*), L-neurofilament (*G*), or α-synuclein (*H*). Means ± S.E. are shown. *, $p < 0.05$ *versus* exGFP or vehicle.

amyloidogenic proteins, APP, and Tau and increased inflammatory signaling lead to apoptosis and neurodegeneration (Fig. 9*B*). Only the initial stages of the proposed hypothesis were confirmed in this study. Accumulation of misfolded amyloidogenic proteins and consequences of this process require models allowing for long-term experiments; such long-term animal experiments will evaluate the contribution of the proposed mechanism to the neurodegenerative process and cognitive impairment. It is important to recognize that exNef may also affect other cell types in the brain, *e.g.* glial cells and macrophages; these cells may contribute to the overall pathology of HAND.

One limitation of this study is that it used SH-SY5Y human neuroblastoma cells as the main *in vitro* model. Although this cell line is frequently used as a model of neurons, its properties are not identical to the primary neuronal cells. Second, transfection of cells with Nef may alter the properties of EVs produced by these cells. However, we previously demonstrated that the effects of EVs produced by Nef-expressing cells are identical to those produced by HIV-infected cells, but not by ΔNefHIV-infected cells, and the effects of Nef EVs on target cells were indistinguishable from the effect of recombinant Nef protein (13), pointing to Nef as the main active factor. Finally, animal and human studies did not differentiate between different brain cell populations, although the analyzed proteins (except for ABCA1) are mainly expressed in the neurons. In conclusion, our findings are consistent with a hypothesis that Nef-containing EVs secreted into CSF by HIV-infected cells in the brain cause impairment of cholesterol metabolism and lipid rafts in neurons, thus contributing to the pathogenesis of HAND.

Experimental procedures

EV production and purification

Nef-containing EVs (exNef) were isolated from cell culture medium of HEK293 cells transfected with Nef. HEK293 cells were transfected with plasmids expressing Nef or GFP using Lipofectamine (Invitrogen) and grown in DMEM containing 10% exosome-depleted FBS for up to 4 days. Medium
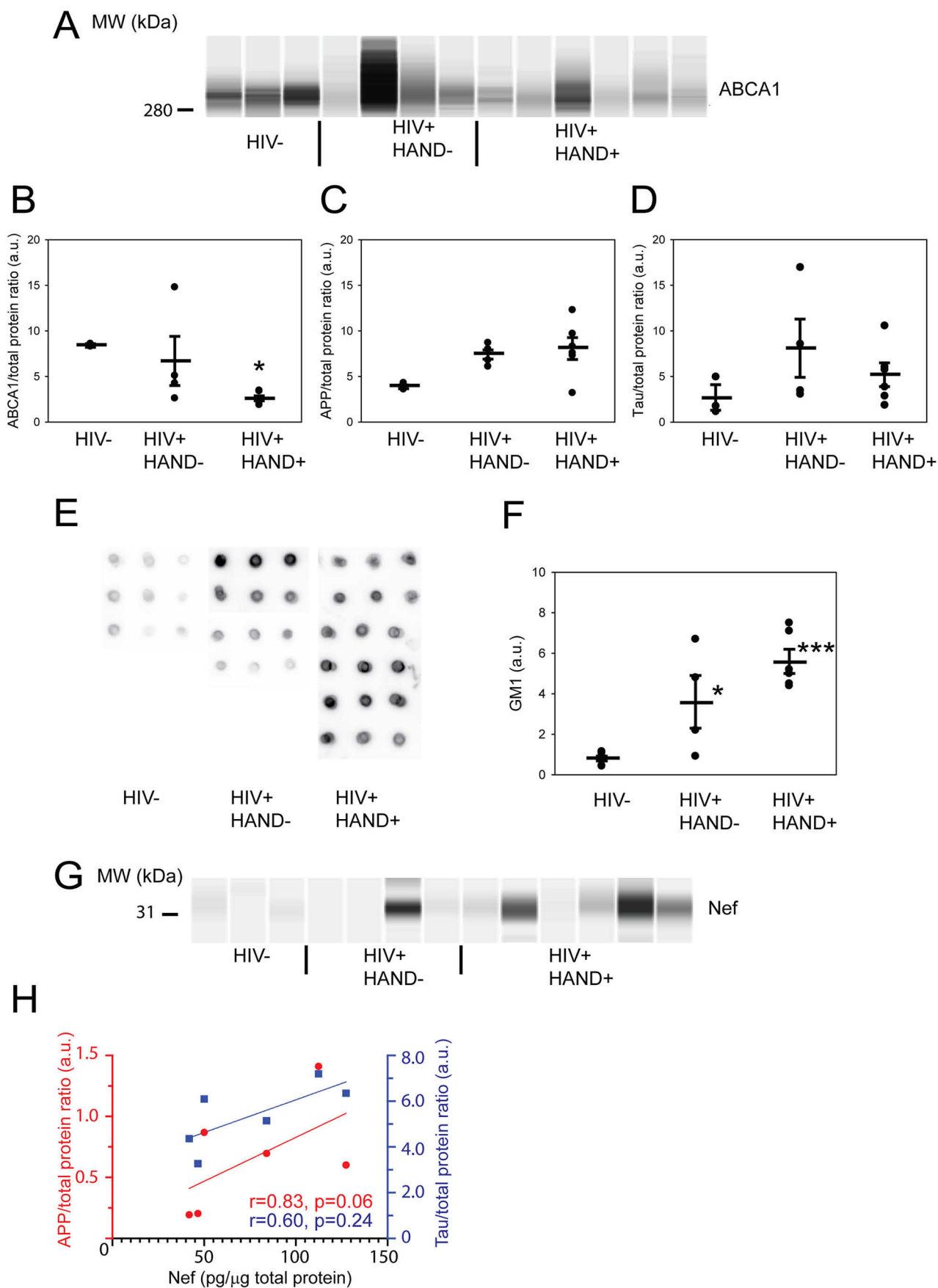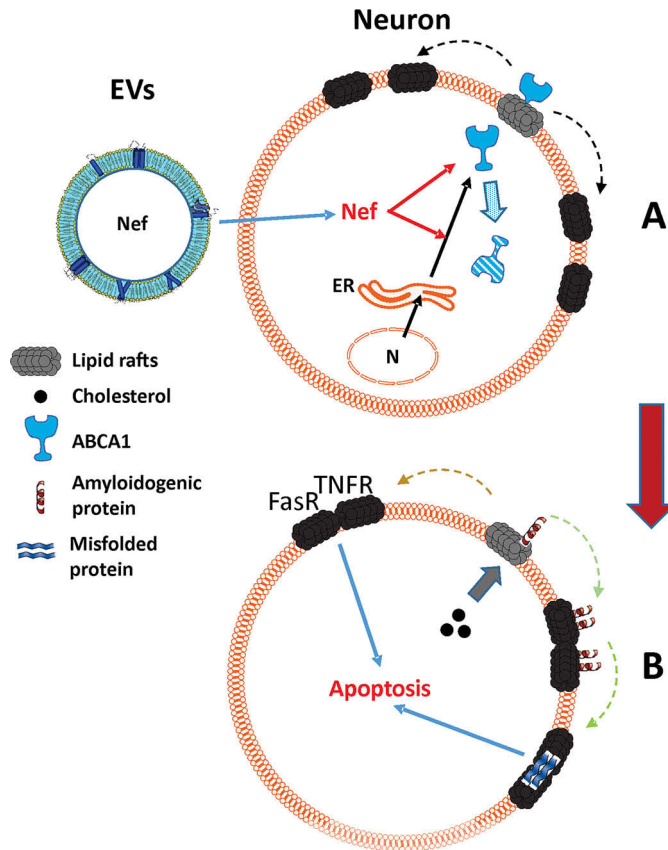
Figure 9. Proposed hypothesis of pathogenesis of HAND. ExNef causes reduction of cellular ABCA1, leading to increased abundance and modification of lipid rafts (*A*). This potentiates accumulation of amyloidogenic proteins, APP, and Tau in modified lipid rafts leading to protein misfolding and aggregation (*B*). Increased abundance and modification of lipid rafts and amyloidogenic protein misfolding exacerbates inflammatory signaling originating from rafts leading to neuroinflammation, apoptosis and neurodegeneration (*B*). *N*, nucleus; *ER*, endoplasmic reticulum; *TNFR*, tumor necrosis factor receptor; *FasR*, Fas receptor.

containing EV was collected and cleared from cells and debris by centrifugation at $300 \times g$ for 10 min and then at $2,000 \times g$ for 20 min. The medium was then combined with PEG6000 (Sigma–Aldrich) solution to a final concentration of 8% PEG, 0.5 M NaCl, incubated with agitation overnight at 4 °C, and centrifuged at $3,200 \times g$ for 1 h. The resulting pellet was twice rinsed with PBS, resuspended, and centrifuged at $100,000 \times g$ for 70 min. The EVs were confirmed to contain Nef or GFP by Western blotting using mouse monoclonal anti-Nef or anti-GFP antibody as described previously (13). Characterization of EVs produced by this method, including size distribution, presence of EV markers, concentration and enrichment with Nef, and presence of coding and noncoding RNAs, was described previously (13, 21). EV concentration was standardized from batch to batch to a known Nef concentration. Exosome-

depleted FBS was obtained by centrifugation of the whole FBS at $300,000 \times g$ at 4 °C for 24 h.

Recombinant Nef

rNef was produced and purified by Monash Protein Production unit (Melbourne, Australia) as previously described (41). The purity of rNef was confirmed by MS. LPS contamination of rNef was assessed using Pierce LAL chromogenic endotoxin quantitation kit and was below 0.01 EU/μg rNef.

Cells and tissues

Human neuroblastoma cells SH-SY5Y (ATCC, Manassas, VA, USA) were maintained in DMEM/F12 medium containing 10% FBS at 37 °C, 5% CO_2. The cells were differentiated as follows. The cells between passages 13 and 25 were seeded onto collagen-coated plates or microscope chamber slides at a density of 2.25×10^3/cm^2. The cells underwent primary differentiation by a 5-day incubation with complete media supplemented with 10 μM retinoic acid (Sigma–Aldrich), followed by a secondary differentiation for 2 days by incubating the cells in serum-free DMEM/F12 medium with 5 ng/ml brain-derived neurotrophic factor (BDNF) (Abcam). The cells were subsequently maintained in serum-free BDNF-containing media. Cell differentiation was confirmed visually by morphologic changes and spread of neurites as well by staining for MAP2. The cells were treated for 48 h with either Nef-containing EVs (exNef; final concentration, 0.4 ng/ml Nef) or GFP-containing EVs (exGFP) added at the equivalent total protein concentration. Where indicated, the cells were treated for the same duration with 100 ng/ml (final concentration) of rNef (refreshed every 24 h) or vehicle.

For lipid raft disruption studies, following treatment with EVs the cells were treated with 0.25 mM of MβCD for 60 min. To assess glutamate-induced excitotoxicity, differentiated cells were treated for 1 h with 50 μM of glutamate.

Brain slices from HIV-infected patients diagnosed or not with neurocognitive impairment were obtained as anonymized samples from NNTC. Anonymized brain tissue samples of uninfected controls were provided by NIH NeuroBioBank.

EV uptake

PKH67 green fluorescent cell linker mini kit (Sigma–Aldrich) was used according to the manufacturer's instructions to label purified EV with PKH67 dye. Briefly, 20 μg of EVs or 20 μg of BSA were combined with diluent to a total of 250 μl and combined with 250 μl of prediluted PKH67 dye. Following a 5-min incubation, the reaction was stopped by the addition of BSA containing solution to the final concentration of 2% BSA. The solution was then transferred to a

Figure 8. Level of ABCA1 is reduced and abundance of APP, Tau, and lipid rafts is increased in brains of patients with HAND. *A*, visualization of the abundances of ABCA1 and total protein in human brain homogenate analyzed with microfluidic capillary immunoassay. *B*, quantitation of the abundance of ABCA1 in brain homogenates from three groups of patients. Means $\pm$ S.E. are shown. *, $p = 0.03$ *versus* HIV-negative group. *C*, quantitation of the abundance of APP in brain homogenates from three groups of patients. Means $\pm$ S.E. are shown. *D*, quantitation of the abundance of Tau in brain homogenates from three groups of patients. Means $\pm$ S.E. are shown. *E*, visualization of the abundances of GM1 (marker of lipid rafts) in human brain homogenate analyzed with dot blot. *F*, quantitation of the abundance of ABCA1 in brain homogenates from three groups of patients. Means $\pm$ S.E. are shown. *, $p < 0.05$; ***, $p < 0.001$ *versus* HIV-negative group. *G*, visualization of the abundance of Nef in human brain homogenate analyzed with microfluidic capillary immunoassay. *H*, correlation between levels of Nef and APP (*red*) or Tau (*blue*). *MW*, molecular mass.

300,000-kDa spin columns (Sartorius) and spun at 15,000 $\times$ *g* for 10 min. Unbound dye was then washed out by repeated centrifugation following the addition of PBS containing 0.1% BSA for the first five washes and PBS alone for all subsequent washes. Dye was considered to be washed out from EVs or BSA when flow through had background levels of fluorescence. Uptake of EVs was assessed following incubation of differentiated SH-SY5Y cells grown on 8-well microscope slides (ibidi) with 2 μg of PKH67 stained BSA or EVs for 1, 2, 3, 6, or 8 h. The cells were then counterstained with Hoechst 33342 (Invitrogen). Fluorescence stain was detected with Nikon A1R using the 40$\times$ water immersion objective. Total stain per cell was calculated using FIJI image processing software. To measure long-term uptake of exNef, the cells were incubated 24–48 h with 5 μg/ml EVs containing GFP-Nef. Intracellular GFP was detected as described below using anti-GFP antibody.

Confocal microscopy

Changes in lipid rafts were detected utilizing Vybrant lipid raft labeling kit (Invitrogen) as per the manufacturer's instructions. Briefly, following treatment(s), the cells were washed once with PBS and fixed with ice-cold 4% paraformaldehyde solution in PBS for 3 min. The cells were then washed twice with PBS and incubated with Alexa 488– or Alexa 647–labeled CTB for 10 min at 4 °C. The cells were then washed twice with PBS, incubated with anti-CTB rabbit antibody for 15 min, and washed two more times before secondary fixation with 4% paraformaldehyde solution in PBS (4 min) followed by further three washing steps. If staining with Tau and APP antibodies was needed, the cells were permeabilized with 0.1% (v/v) Triton X-100 for 3 min at 4 °C, blocked with 10% (v/v) goat serum for 30 min, and incubated with anti-Tau mouse monoclonal or anti-APP mouse monoclonal antibodies. Antibody binding was detected with either goat anti-mouse Alexa 488 or goat anti-mouse Alexa 647 (Invitrogen). The cells were then counterstained with Hoechst 33342 and imaged as described above. For lipid raft analysis by flow cytometry (FACS Canto II (BD bioscience)), cells were scraped after secondary fixation, centrifuged at 300 $\times$ *g*, and resuspended in 150 μl of PBS with 0.1% BSA.

Lipid raft isolation

Lipid rafts were isolated from a postnuclear supernatant by flotation through a continuous OptiPrep (Sigma–Aldrich) density gradient. For detection of rafts in some experiments, cellular cholesterol in SH-SY5Y cells was labeled with [1α,2α (n)-^{3}H]cholesterol] (GE Healthcare) at 0.1 μCi/ml for 24 h. Briefly, the cells were washed with ice-cold PBS, collected, and treated with 5 mM Tris-HCl buffer (pH 7.5) containing a complete mixture of protease/phosphatase inhibitors (Roche). Postnuclear fraction was prepared by hypo-osmotic shock followed with repeated freezing-thawing. Cellular debris was spun down at 300 $\times$ *g* for 5 min at 4 °C; supernatant was collected and spun at 100,000 $\times$ *g* 90 min at 4 °C; and the resulting pellet was resuspended in 23% iodixanol solution containing protease/phosphatase inhibitors. OptiPrep 10–20% linear gradient was

formed using standard two-chamber gradient maker, and the samples were underlayered. After the first centrifugation (52,000 $\times$ *g* for 90 min in swing-bucket rotor), the top part of the tube content (40%) was collected and transferred to another tube. 15 and 5% of iodixanol were layered over the samples and centrifuged at 52,000 $\times$ *g* for 90 min. 50-μl fractions were collected from the top and processed either for radioactivity counting and/or flotillin-1 detection by Western blotting.

Cholesterol efflux

Cholesterol efflux was performed as previously described (42) with minor modifications. Cellular cholesterol in SH-SY5Y cells was labeled with [1α,2α (n)-^{3}H]cholesterol] at 0.5 μCi/ml for 48 h at the end of primary differentiation stage. The cells were then washed twice before the secondary differentiation and underwent treatment as per usual procedure. During the last day of treatment, the cells were supplemented with LXR agonist TO-901317 (4 μmol/liter) for 18 h. The cells were then washed and incubated for 2 h at 37 °C in BDNF-containing serum-free media containing 20 μg/ml of purified human apolipoprotein A-I (a gift from the Commonwealth Serum Laboratory). Subsequently, the medium was collected, the cells were lysed by two cycles of freeze-thawing in a distilled H_2O, and [^{3}H]cholesterol content was assessed with Hidex 600SL scintillation counter. Cholesterol efflux was expressed as a ratio of [^{3}H]cholesterol in the media to total [^{3}H]cholesterol amount. Nonspecific efflux (*i.e.* the efflux in the absence of an acceptor) was then subtracted.

Western blotting and dot blot

Cultured cells or mouse brain homogenates were lysed in radioimmune precipitation assay buffer supplemented with protease/phosphatase inhibitor mixture. The lysates were then separated on an SDS-PAGE, transferred to PVDF or nitrocellulose membrane, and, following a block in 4% skim milk, probed with different antibodies. Staining was detected using Lighting ECL (PerkinElmer). The images were taken and quantitated using GBox (Syngene).

Human brain homogenates were prepared as described above and analyzed with ProteinSimple (San Jose, CA) Jess microfluidic capillary immunoassay, using manufacturer's software (AlphaView) for band quantification. Loading control for quantification was total protein measured in the same capillary as the protein of interest, using ProteinSimple proprietary technology. The same homogenates were analyzed for GM1 abundance using dot blot. In brief, 2 μl of each sample was blotted on a nitrocellulose membrane, which was dried at room temperature, blocked with 1$\times$ KPL detector block (SeraCare Life Sciences, Milford, MA, USA) for 1 h, and probed with CTB-HRP (1 μg/ml) in blocking buffer for 1 h at room temperature, washed, and imaged using FluoroChem R System (ProteinSimple).

The sources of the antibodies were as follows. Mouse monoclonal anti–β-amyloid/APP mouse antibody (catalog no. sc-28365) was from Santa Cruz Biotechnology. Rabbit polyclonal anti-APP (for capillary immunoassay, catalog no.

NBP1-76910) was from Novus Biologicals. Rabbit monoclonal anti-β-amyloid antibody (catalog no. 8243S), mouse monoclonal anti-Tau antibody (catalog no. 4019S), mouse monoclonal anti-phosphorylated Tau antibody (catalog no. 9632S), mouse monoclonal anti-α-synuclein antibody (catalog no. 2647S), rabbit monoclonal anti–neurofilament-L antibody (catalog no. 2837S), rabbit monoclonal anti-phosphorylated ERK1/2 antibody (catalog no. 4370S), rabbit polyclonal anti-p38 MAPK (catalog no. 9212S), mouse monoclonal anti-phosphorylated p38 MAPK (Thr^{180}/Tyr^{182}, catalog no. 9216S), anti-mouse IgG (catalog no. 7076S), and anti-rabbit IgG horseradish peroxidase conjugates (catalog no. 7074S) were from Cell Signaling Technologies. Mouse monoclonal anti-ABCA1 antibody (catalog no. ab18180) and mouse monoclonal anti–sodium potassium ATPase antibody (catalog no. ab7671) were from Abcam. Mouse monoclonal anti-GAPDH antibody (catalog no. CB1001) and mouse monoclonal anti-ERK1/2 antibody (catalog no. 05-1152) were from Merck. Mouse monoclonal anti-Nef antibody was obtained through the National Institutes of Health AIDS Reagent Program, Division of AIDS, NIAID, National Institutes of Health (anti-HIV-1 SF2 Nef monoclonal antibody, EH1, catalog no. 3689). The antibody used for capillary immunoassay was a kind gift from Dr. Matthias Clauss (Indiana University and Purdue University, Indianapolis, IN, USA).

Amyloid β_{42} ELISA

Human Aβ_{42} ELISA kit (Invitrogen) was used to estimate amyloid β_{42} in cells and cell culture supernatant. Cell culture media and cell lysates were collected. To prevent amyloid β_{42} degradation by serine proteases, 4-(2-aminoethyl) benzenesulfonyl fluoride (1 mM) was added into each sample. ELISA was performed according to manufacturer's protocol.

Apoptosis and necrosis

Apoptosis and necrosis was assessed using cell death detection ELISA kit (Roche) as reported previously (43). For glutamate-induced excitotoxicity experiments, cell death ELISA results were confirmed via propidium iodide incorporation. Briefly cells grown on microscope slides (ibidi) and treated with glutamate were supplemented with 5 mM propidium iodide for last 30 min of glutamate treatment. The cells were then washed, fixed for 5 min in 4% paraformaldehyde in PBS counterstained with Hoechst 33342 (Invitrogen), and imaged using Nikon A1R. The percentage of dead cells per microscope field of view was then calculated for at least 30 randomly selected fields per treatment.

Acetylcholinesterase assay

Acetylcholinesterase assay was performed using a colorimetric kit (Abcam) as per the manufacturer's instructions. Acetylcholinesterase activity was adjusted to the sample's protein content.

Animal studies

C57BL/J6 mice were bread at the Alfred Research Alliance Animal Centre. The mice were maintained on normal chow throughout the experimental procedure. To test the effect of rNef, 12 male mice at 8 weeks of age were divided into two groups of 6 mice and treated for 9 days with either PBS or rNef (50 ng in 100 μl of PBS per injection) via intravenous injections every 2 days. 18 mice were used to study the effect of exNef on the brains. The mice were divided into two groups of 9 mice, and exNef or exGFP (2 μg of total EV protein in 100 μl of PBS per injection) was administered every 3 days via intravenous injections for 14 days. The mice were then euthanized by CO_2 inhalation. The mouse brains were dissected out and divided into two hemispheres: one hemisphere was homogenized in PBS supplemented with protease/phosphatase inhibitor mixture and divided into individual aliquots before freezing in liquid nitrogen for subsequent analysis.

All animal experiments were approved by the Animal Ethics Committee of the Alfred Research Alliance (approval no. 6553) and conducted in accordance with the Australian Code of Practice for the Care and Use of Animals for Scientific Purposes as stipulated by the National Health and Medical Research Council of Australia. All mice were housed in a normal light and dark cycle and had *ad libitum* access to food and water. The mice were randomly assigned to treatment.

Human brain tissues

Frozen brain tissues were obtained from NNTC and the National Institutes of Health NeuroBioBank. All samples were anonymized, information about the clinical status of donors was provided by NNTC. The studies abided by the Declaration of Helsinki principles.

Statistics

All data are shown as means $\pm$ S.E. GraphPad and R software packages were used to examine the data for statistical significance between groups. Student's t test or analysis of variance with Tukey adjustment for multiple comparisons were used when data followed a normal distribution; alternatively, a Mann–Whitney test on ranks was used.

Data availability

All of the data generated during this study are included in this published article.

Author contributions—M. D., H. L., A. J. M., and D. S. data curation; M. D., T. P., A. J. M., and D. S. formal analysis; M. D., A. J. M., and

Abbreviations—The abbreviations used are: HAND, HIV-associated neurocognitive disorder; APP, amyloid precursor protein; NNTC, National NeuroAIDS Tissue Consortium; PLWH, people living with HIV; AD, Alzheimer's disease; EV, extracellular vesicle; CSF, cerebrospinal fluid; ART, anti-retroviral therapy; CTB, cholera toxin subunit B; AChE, acetylcholine esterase; MβCD, methyl-β-cyclodextrin; DMEM, Dulbecco's modified Eagle's medium; FBS, fetal bovine serum; rNef, recombinant myristoylated Nef; BDNF, brain-derived neurotrophic factor; GAPDH, glyceraldehyde-3-phosphate dehydrogenase.

References

1. Saylor, D., Dickens, A. M., Sacktor, N., Haughey, N., Slusher, B., Pletnikov, M., Mankowski, J. L., Brown, A., Volsky, D. J., and McArthur, J. C. (2016) HIV-associated neurocognitive disorder: pathogenesis and prospects for treatment. *Nat. Rev. Neurol.* **12,** 234–248 CrossRef Medline

2. Antinori, A., Arendt, G., Becker, J. T., Brew, B. J., Byrd, D. A., Cherner, M., Clifford, D. B., Cinque, P., Epstein, L. G., Goodkin, K., Gisslen, M., Grant, I., Heaton, R. K., Joseph, J., Marder, K., *et al.* (2007) Updated research nosology for HIV-associated neurocognitive disorders. *Neurology* **69,** 1789–1799 CrossRef Medline

3. Cysique, L. A., and Brew, B. J. (2011) Prevalence of non-confounded HIV-associated neurocognitive impairment in the context of plasma HIV RNA suppression. *J. Neurovirol.* **17,** 176–183 CrossRef Medline

4. Brew, B. J., Crowe, S. M., Landay, A., Cysique, L. A., and Guillemin, G. (2009) Neurodegeneration and ageing in the HAART era. *J. Neuroimmune Pharmacol.* **4,** 163–174 CrossRef Medline

5. Schengrund, C. L. (2010) Lipid rafts: keys to neurodegeneration. *Brain. Res. Bull.* **82,** 7–17 CrossRef Medline

6. Björkhem, I., Leoni, V., and Meaney, S. (2010) Genetic connections between neurological disorders and cholesterol metabolism. *J. Lipid Res.* **51,** 2489–2503 CrossRef Medline

7. Grassi, S., Giussani, P., Mauri, L., Prioni, S., Sonnino, S., and Prinetti, A. (2020) Lipid rafts and neurodegeneration: structural and functional roles in physiologic aging and neurodegenerative diseases. *J. Lipid Res.* **61,** 636–654 CrossRef Medline

8. Sonnino, S., Aureli, M., Grassi, S., Mauri, L., Prioni, S., and Prinetti, A. (2014) Lipid rafts in neurodegeneration and neuroprotection. *Mol. Neurobiol.* **50,** 130–148 CrossRef Medline

9. Waheed, A. A., and Freed, E. O. (2009) Lipids and membrane microdomains in HIV-1 replication. *Virus Res.* **143,** 162–176 CrossRef Medline

10. Mujawar, Z., Rose, H., Morrow, M. P., Pushkarsky, T., Dubrovsky, L., Mukhamedova, N., Fu, Y., Dart, A., Orenstein, J. M., Bobryshev, Y. V., Bukrinsky, M., and Sviridov, D. (2006) Human immunodeficiency virus impairs reverse cholesterol transport from macrophages. *PLos Biol.* **4,** e365 CrossRef Medline

11. Cui, H. L., Guo, B., Scicluna, B., Coleman, B. M., Lawson, V. A., Ellett, L., Meikle, P. J., Bukrinsky, M., Mukhamedova, N., Sviridov, D., and Hill, A. F. (2014) Prion infection impairs cholesterol metabolism in neuronal cells. *J. Biol. Chem.* **289,** 789–802 CrossRef Medline

12. Cui, H. L., Ditiatkovski, M., Kesani, R., Bobryshev, Y. V., Liu, Y., Geyer, M., Mukhamedova, N., Bukrinsky, M., and Sviridov, D. (2014) HIV protein Nef causes dyslipidemia and formation of foam cells in mouse models of atherosclerosis. *FASEB J.* **28,** 2828–2839 CrossRef Medline

13. Mukhamedova, N., Hoang, A., Dragoljevic, D., Dubrovsky, L., Pushkarsky, T., Low, H., Ditiatkovski, M., Fu, Y., Ohkawa, R., Meikle, P. J., Horvath, A., Brichacek, B., Miller, Y. I., Murphy, A., Bukrinsky, M., *et al.* (2019) Exosomes containing HIV protein Nef reorganize lipid rafts potentiating inflammatory response in bystander cells. *PLoS Pathog.* **15,** e1007907 CrossRef Medline

14. Lee, J. H., Schierer, S., Blume, K., Dindorf, J., Wittki, S., Xiang, W., Ostalecki, C., Koliha, N., Wild, S., Schuler, G., Fackler, O. T., Saksela, K., Harrer, T., and Baur, A. S. (2016) HIV-Nef and ADAM17-containing plasma extracellular vesicles induce and correlate with immune pathogenesis in chronic HIV infection. *EBioMedicine* **6,** 103–113 CrossRef Medline

15. Ferdin, J., Goricar, K., Dolzan, V., Plemenitas, A., Martin, J. N., Peterlin, B. M., Deeks, S. G., and Lenassi, M. (2018) Viral protein Nef is detected in plasma of half of HIV-infected adults with undetectable plasma HIV RNA. *PLoS One* **13,** e0191613 CrossRef Medline

16. Raymond, A. D., Campbell-Sims, T. C., Khan, M., Lang, M., Huang, M. B., Bond, V. C., and Powell, M. D. (2011) HIV Type 1 Nef is released from infected cells in CD45⁺ microvesicles and is present in the plasma of HIV-infected individuals. *AIDS Res. Hum. Retroviruses* **27,** 167–178 CrossRef Medline

17. Saribas, A. S., Cicalese, S., Ahooyi, T. M., Khalili, K., Amini, S., and Sariyer, I. K. (2017) HIV-1 Nef is released in extracellular vesicles derived from astrocytes: evidence for Nef-mediated neurotoxicity. *Cell Death Dis.* **8,** e2542 CrossRef Medline

18. Raymond, A. D., Diaz, P., Chevelon, S., Agudelo, M., Yndart-Arias, A., Ding, H., Kaushik, A., Jayant, R. D., Nikkhah-Moshaie, R., Roy, U., Pilakka-Kanthikeel, S., and Nair, M. P. (2016) Microglia-derived HIV Nef+ exosome impairment of the blood–brain barrier is treatable by nanomedicine-based delivery of Nef peptides. *J. Neurovirol.* **22,** 129–139 CrossRef Medline

19. Fujii, Y., Otake, K., Tashiro, M., and Adachi, A. (1996) Soluble Nef antigen of HIV-1 is cytotoxic for human CD4+ T cells. *FEBS Lett.* **393,** 93–96 CrossRef Medline

20. Khan, M. B., Lang, M. J., Huang, M. B., Raymond, A., Bond, V. C., Shiramizu, B., and Powell, M. D. (2016) Nef exosomes isolated from the plasma of individuals with HIV-associated dementia (HAD) can induce Aβ1-42 secretion in SH-SY5Y neural cells. *J. Neurovirol.* **22,** 179–190 CrossRef Medline

21. Dubrovsky, L., Ward, A., Choi, S.-H., Pushkarsky, T., Brichacek, B., Vanpouille, C., Adzhubei, A. A., Mukhamedova, N., Sviridov, D., Margolis, L., Jones, R. B., Miller, Y. I., and Bukrinsky, M. (2020) Inhibition of HIV replication by apolipoprotein A-I binding protein targeting the lipid rafts. *mBio* **11,** e02956-19 Medline

22. Théry, C., Witwer, K. W., Aikawa, E., Alcaraz, M. J., Anderson, J. D., Andriantsitohaina, R., Antoniou, A., Arab, T., Archer, F., Atkin-Smith, G. K., Ayre, D. C., Bach, J.-M., Bachurski, D., Baharvand, H., Balaj, L., *et al.* (2018) Minimal information for studies of extracellular vesicles 2018 (MISEV2018): a position statement of the International Society for Extracellular Vesicles and update of the MISEV2014 guidelines. *J. Extracell. Vesicles* **7,** 1535750 CrossRef Medline

23. Raymond, A. D., Lang, M. J., Chu, J., Campbell-Sims, T., Khan, M., Bond, V. C., Pollard, R. B., Asmuth, D. M., and Powell, M. D. (2019) Plasma-

derived HIV Nef+ exosomes persist in ACTG384 study participants despite successful virological suppression. *bioRxiv* CrossRef

24. Stoothoff, W. H., and Johnson, G. V. (2005) Tau phosphorylation: physiological and pathological consequences. *Biochim. Biophys. Acta* **1739,** 280–297 CrossRef Medline

25. Alonso, A. C., Zaidi, T., Grundke-Iqbal, I., and Iqbal, K. (1994) Role of abnormally phosphorylated Tau in the breakdown of microtubules in Alzheimer disease. *Proc. Natl. Acad. Sci. U.S.A.* **91,** 5562–5566 CrossRef Medline

26. Qi, H., Prabakaran, S., Cantrelle, F.-X., Chambraud, B., Gunawardena, J., Lippens, G., and Landrieu, I. (2016) Characterization of neuronal Tau protein as a target of extracellular signal–regulated kinase. *J. Biol. Chem.* **291,** 7742–7753 CrossRef Medline

27. Costes, S. V., Daelemans, D., Cho, E. H., Dobbin, Z., Pavlakis, G., and Lockett, S. (2004) Automatic and quantitative measurement of protein–protein colocalization in live cells. *Biophys. J.* **86,** 3993–4003 CrossRef Medline

28. Choi, D. W. (1992) Excitotoxic cell death. *J. Neurobiol.* **23,** 1261–1276 CrossRef Medline

29. Tzschentke, T. M. (2002) Glutamatergic mechanisms in different disease states: overview and therapeutical implications: an introduction. *Amino Acids* **23,** 147–152 CrossRef Medline

30. Madhusudan, A., Sidler, C., and Knuesel, I. (2009) Accumulation of reelin-positive plaques is accompanied by a decline in basal forebrain projection neurons during normal aging. *Eur. J. Neurosci.* **30,** 1064–1076 CrossRef Medline

31. Zidovetzki, R., and Levitan, I. (2007) Use of cyclodextrins to manipulate plasma membrane cholesterol content: evidence, misconceptions and control strategies. *Biochim. Biophys. Acta* **1768,** 1311–1324 CrossRef Medline

32. Wong, M. E., Jaworowski, A., and Hearps, A. C. (2019) The HIV reservoir in monocytes and macrophages. *Front. Immunol.* **10,** 1435 CrossRef Medline

33. Furler, R. L., and Uittenbogaart, C. H. (2010) Signaling through the P38 and ERK pathways: a common link between HIV replication and the immune response. *Immunol. Res.* **48,** 99–109 CrossRef Medline

34. Saeedi, S., Israel, S., Nagy, C., and Turecki, G. (2019) The emerging role of exosomes in mental disorders. *Transl. Psychiatry* **9,** 122 CrossRef Medline

35. Kaul, M. (2008) HIV's double strike at the brain: neuronal toxicity and compromised neurogenesis. *Front. Biosci.* **13,** 2484–2494 CrossRef Medline

36. Sorci-Thomas, M. G., and Thomas, M. J. (2016) Microdomains, inflammation, and atherosclerosis. *Circ. Res.* **118,** 679–691 CrossRef Medline

37. Lamers, S. L., Fogel, G. B., Liu, E. S., Barbier, A. E., Rodriguez, C. W., Singer, E. J., Nolan, D. J., Rose, R., and McGrath, M. S. (2018) Brain-specific HIV Nef identified in multiple patients with neurological disease. *J. Neurovirol.* **24,** 1–15 CrossRef Medline

38. Ito, A., Hong, C., Rong, X., Zhu, X., Tarling, E. J., Hedde, P. N., Gratton, E., Parks, J., and Tontonoz, P. (2015) LXRs link metabolism to inflammation through Abca1-dependent regulation of membrane composition and TLR signaling. *eLife* **4,** e08009 CrossRef Medline

39. Borjabad, A., and Volsky, D. J. (2012) Common transcriptional signatures in brain tissue from patients with HIV-associated neurocognitive disorders, Alzheimer's disease, and multiple sclerosis. *J. Neuroimmune Pharmacol.* **7,** 914–926 CrossRef Medline

40. Fulop, T., Witkowski, J. M., Larbi, A., Khalil, A., Herbein, G., and Frost, E. H. (2019) Does HIV infection contribute to increased β-amyloid synthesis and plaque formation leading to neurodegeneration and Alzheimer's disease? *J. Neurovirol.* **25,** 634–647 CrossRef Medline

41. Glück, J. M., Hoffmann, S., Koenig, B. W., and Willbold, D. (2010) Single vector system for efficient *N*-myristoylation of recombinant proteins in *E. coli. PLoS One* **5,** e10081 CrossRef Medline

42. Low, H., Hoang, A., and Sviridov, D. (2012) Cholesterol efflux assay. *J. Vis. Exp.* e3810 Medline

43. Low, H., Mukhamedova, N., Cui, H. L., McSharry, B. P., Avdic, S., Hoang, A., Ditiatkovski, M., Liu, Y., Fu, Y., Meikle, P. J., Blomberg, M., Polyzos, K. A., Miller, W. E., Religa, P., Bukrinsky, M., *et al.* (2016) Cytomegalovirus restructures lipid rafts via a US28/CDC42-mediated pathway, enhancing cholesterol efflux from host cells. *Cell Rep.* **16,** 186–200 CrossRef Medline